Comparison of the Growth Patterns of Si_n and Ge_n Clusters ($n = 25-33$)

Li-Zhen Zhao,[†] Wen-Cai Lu,*[,†,‡] and Wei Qin[†]

State Key Laboratory of Theoretical and Computational Chemistry, Institute of Theoretical Chemistry, Jilin University, Changchun, Jilin 130021, People's Republic of China, and Department of Physics, Qingdao University, Qingdao, Shandong 266071, People's Republic of China

C. Z. Wang and K. M. Ho

Ames Laboratory—U.S. DOE and Department of Physics and Astronomy, Iowa State University, Ames, Iowa 50011

Received: November 16, 2007; Revised Manuscript Received: March 7, 2008

We performed an unbiased search for low-energy structures of medium-sized neutral Si_n and Ge_n clusters ($n = 25-33$) using a genetic algorithm (GA) coupled with tight-binding interatomic potentials. Structural candidates obtained from our GA search were further optimized by first-principles calculations using density functional theory (DFT). Our approach reproduces well the lowest-energy structures of Si_n and Ge_n clusters of $n = 25-29$ compared to previous studies, showing the accuracy and reliability of our approach. In the present study, we pay more attention to determine low-lying isomers of Si_n and Ge_n ($n = 29-33$) and study the growth patterns of these clusters. The B3LYP calculations suggest that the growth pattern of Si_n ($n = 25-33$) clusters undergoes a transition from prolate to cage at $n = 31$, while this transition appears at $n = 26$ from the PBE-calculated results. In the size range of 25−33, the corresponding Ge_n clusters hold the prolate growth pattern. The relative stabilities and different structural motifs of Si_n and Ge_n ($n = 25-33$) clusters were studied, and the changes of small cluster structures, when acting as building blocks of large clusters, were also discussed.

I. Introduction

During the past several decades, cluster science has been undergoing intensive development. Cluster research is primarily driven by the interest in evolution of the structures and properties of materials from molecular to macroscopic systems. In particular, semiconductor clusters have been extensively investigated by both experimental[1–23] and theoretical[24–39] approaches because of their potential applications in the microelectronics industry. Since silicon and germanium are two important materials in microelectronics applications, understanding the growth mechanisms of these materials at the cluster regime is of great interest. As a bridge between small clusters and nanoparticles, the medium-sized Si_n and Ge_n ($n = 20-100$) clusters have attracted much attention.[24–34]

Knowledge of the geometric structures of low-energy clusters is important to the understanding of structural evolution and change in electronic properties as the size of a cluster grows. Physical properties of some silicon and germanium clusters such as atomization energies,[1] mass spectra,[2–4]photofragmentation,[5] photoionization,[6,21–23] photoelectron spectroscopy,[7] electronic gap,[12] polarizability,[17] and chemical reactivity obtained from experiments[9,13–15,21] suggested that the structures of silicon and germanium clusters are very much the same at small sizes ($n \leq 12$). However, ion mobility measurements revealed a significant structural difference when the size increases to 25.[8,16,19,20] While the shapes of Si_n clusters show a transition from prolate to near-spherical in the size range 24−34,[16,19,20] near-spherical Ge_n clusters do not show it until $n = 64-76$.[8]

In the size range $13 \leq n \leq 20$, although the growth patterns of many silicon clusters differ from those of germanium clusters,[10,35] a majority of low-lying silicon and germanium clusters still contain two common structural motifs, namely, the TTP (tricapped trigonal prism) motif and the six/six (a puckered-hexagonal ring attached to a tetragonal bipyramid Si_6 or Ge_6) motif.

There have been more studies for the low-energy structures of silicon clusters than for those of germanium clusters in the size range $n \geq 21$. Using the density functional based tight-binding (DFTB) potential for Si, Jackson et al.[27] have investigated the structures of Si_{25}, Si_{29}, and Si_{35} by a molecular-dynamics simulated annealing method and revealed the shape transition sketchily. Recently they employed a big bang search scheme to obtain some structures for silicon clusters with 20−27 atoms.[28] These structures neither resemble bulk silicon packing nor obey the rule of TTP stacking. Yoo et al.[29] used a combined molecular mechanics−quantum mechanics procedure to search for Si_{21} and Si_{25} clusters. They found some isomers that have appreciably lower energy than those reported previously. They have also constructed the stuffed-fullerene clusters and obtained more spherical-like Si_n geometric structures in the size range 27−39 using a genetic algorithm combined with the tight-binding method.[30] Wang et al.[31] have reported a combined study of photoelectron spectroscopy and first-principles DFT calculations of Si_n clusters in the size range $20 \leq n \leq 45$, and suggested that there is a transition from prolate to near-spherical structure at $n = 27$. Very recently Yoo and co-workers,[32,33] have performed an unconstrained search for low-lying structures of medium-sized silicon clusters $Si_{21}-Si_{40}$ and Si_{45}, by means of the minimum-hopping global optimization method coupled with a density functional based tight-binding (DFTB) model of

* Corresponding author. E-mail: wencailu@jlu.edu.cn.
† Jilin University.
‡ Qingdao University.

10.1021/jp710937m CCC: $40.75
Published on Web 06/06/2008

silicon, followed by further structure optimization using first-principles DFT calculations to determine the relative stability of various candidates of low-lying silicon clusters. They proposed that all the low-lying clusters can be classified into four structural families, indicating four growth patterns. Oña et al. employed a genetic algorithm with the MSINDO semiempirical molecular orbital program to search for stable structures in the size range $Si_{18}-Si_{60}$ and further optimized them with the DFT method.[34] They reported many structures with lower energies that are different from the previous studies, which indicates that the structures of medium-sized silicon clusters are still under much debate.

In contrast with the studies of silicon clusters, many fewer studies have been devoted to the germanium clusters in this size range. Candidate structures for lowest-energy Ge_n clusters up to $n = 25$ were investigated by Wang et al.[36] using the genetic algorithm (GA) coupled with a nonorthogonal tight-binding (NTB) model. They found that the stacked layered structures and the spherical-like compact structures compete for the lowest-energy structures for Ge_n ($n > 13$). Recently they employed the same method and obtained the lowest-energy structures of Ge_n clusters up to ~40 atoms,[37] and found the structural change from cage-like to two shell structures around $n = 19$. Liang and Li[38] studied geometric structures and electronic properties of medium-sized clusters Ge_n ($21 \leq n \leq 25$) using a full-potential linear-muffin-tin-orbital molecular-dynamics (FP-LMTO-MD) method. They suggested that low-lying prolate clusters can be built upon stacked TTP motifs. Very recently Yoo and Zeng[39] reported the geometries of low-lying neutral germanium clusters Ge_n ($21 \leq n \leq 29$), based on a basin-hopping global optimization method. They suggested that most low-lying clusters consist of the six/nine and six/ten motifs (a puckered-hexagonal ring unit attached to Ge_9 or Ge_{10}).

Experimental and theoretical studies have revealed that the growth patterns of silicon and germanium clusters are much different from each other around $n = 30$. In this work we examine the structures and relative stabilities of those low-lying silicon and germanium clusters in the size range $25 \leq n \leq 33$; our purpose is to better understand the growth pattern deviation of medium-sized silicon and germanium clusters around $n = 30$. We performed an unbiased global search for the ground-state structures of silicon and germanium clusters using a genetic algorithm (GA) coupled with a tight-binding (TB) interatomic potential with sizes ranging from $n = 25$ to $n = 33$ atoms. Low-energy candidates obtained from the GA/TB search are further optimized with the DFT method. As the size of the cluster increases, the search for the true global minima becomes increasingly challenging. Nevertheless, the unbiased global search based on the GA/TB method is very effective, which allows us to search for a larger structure phase space. By combining the GA/TB search with DFT calculations, we have successfully determined the lower-energy structures of Si_n and Ge_n ($n = 25-33$) clusters. The lowest-energy structures of Si_n ($n = 25-33$) and Ge_n ($n = 25-29$) obtained from our approach are consistent with those previously reported.[31–34,39]The low-energy isomers of Ge_n ($n = 30-33$) presented in this paper are new. The growth patterns of Si_n and Ge_n with $25 \leq n \leq 33$ are compared.

II. Computational Method

The entire computation process can be roughly divided into two steps: GA search and DFT optimization. The genetic algorithm calculations in the present study proceed as follows: In generation zero, a population pool of $p = 20$ structures for a given cluster size n is generated by putting n atoms randomly in a simulation cubic box of an appropriate length. The structures are relaxed to their local minima using a tight-binding potential with the steepest descent method. In each subsequent generation, four parents are picked up from the pool and offspring structures are generated by mating the lower half of parent A with the upper half of parent B or the upper half of parent A with the lower half of parent B. Then, 12 offspring structures are relaxed to their local minima with the TB method. The population pool is updated if the new structure has lower energy and is different from the structures in the pool. The genetic algorithm calculations proceeded up to 1000 generations.

At the end of the global minimum structure search, as many as $p = 20$ structures remain as possible candidates. For Si_n, the selected candidates were further optimized using two DFT methods: (1) the B3LYP functional with a 6-31G(d) basis set in the Gaussian 03 package;[40] (2) the PBE functional with a DND basis set (double numerical basis plus *d*-polarization function) in DMol3 of Materials Studio Package.[41] For Ge_n, we performed our calculations with the PBE/DND method using DMol3. In the DFT calculations, the structures were fully optimized without any symmetry constraint. We have also performed frequency calculations for all the lowest-energy Si_n and Ge_n structures which are confirmed to be energy minimum structures.

We have examined the effects of different exchange-correlation energy functionals and different basis sets using the DFT calculations on the relative energetic stabilities of various isomers of silicon and germanium clusters. We found that while the general trend of the growth motif is not sensitive to the choice of the energy functional and basis set, the spherical motif of silicon clusters appears earlier when the DMol3−PBE instead of the Gaussian 03−B3LYP package is used. Taking Si_{29} and Ge_{29} as examples, it is found that BLYP/6-31G(d), BLYP/DND, and B3LYP/6-31G(d) calculations predict the same prolate isomer as the lowest-energy structure of Si_{29}, while the BPBE/6-31G(d) and PBE/DND calculations prefer an endohedral cage isomer. The prolate-to-spherical transition in silicon clusters predicted by B3LYP and PBE is at $n = 26$ and 31, respectively; both are in the experimental prediction range of 24–34.[19] For Ge_{29}, both PBE/DND and BLYP/DND calculations predict the same prolate structure as the lowest-energy isomer. Different basis sets under the same functional result in the same lowest-energy isomers for silicon and germanium clusters.

In order to further determine which energy functional is more accurate for silicon or germanium clusters, we have compared the ionization potentials (IPs) calculated with different functionals with the experimental values[22,23] for small Si_n and Ge_n ($n = 5$, 6, 7, 8, 9, and 10) clusters. As shown in Table 1, the IPs of small silicon clusters calculated using B3LYP are closer to the experimental results[22] than those from PBE calculations. On the other hand, for germanium clusters, the PBE-calculated IPs are closer to the experimental results[23] than the BLYP-calculated ones. These comparisons suggest that the B3LYP functional might be more accurate for silicon clusters, while the PBE functional might be more applicable to germanium clusters.

According to these tests, we employed in this work two different functionals (B3LYP in Gaussian 03 and PBE in DMol3) for silicon clusters and only the PBE functional in DMol3 for germanium clusters. As for basis sets, we used a 6-31G(d) basis for the B3LYP method in Gaussian 03, and a DND basis for the PBE method in DMol3. In the following sections, we will discuss silicon clusters based on the B3LYP-

TABLE 1: Ionization Potentials of Small Silicon and Germanium Clusters

	IP (eV)				IP (eV)		
	Gaussian 03/B3LYP/6-31G(d)	DMol3/PBE/DND	expt[a]		DMol3/PBE/DND	DMol3/BLYP/DND	expt[b]
Si_5	8.015	7.851	7.97–8.49	Ge_5	7.387	7.094	7.46–7.58
Si_6	7.593	7.375	7.90	Ge_6	7.133	6.891	7.06–7.24
Si_7	7.782	7.685	7.90	Ge_7	7.246	6.922	7.06–7.24
Si_8	7.206	7.020	7.46–7.87	Ge_8	6.532	6.241	6.29–6.36
Si_9	7.465	7.288	7.46–7.87	Ge_9	6.624	6.305	6.55–6.72
Si_{10}	7.676	7.536	7.90	Ge_{10}	6.895	6.533	6.72–6.94

[a] Reference 22. [b] Reference 23.

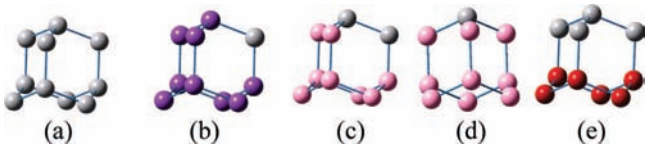

Figure 1. Bulk fragments cut from Si/Ge diamond structure. (a) A bulk fragment with ten atoms; (b) a nine-atom bulk fragment, shown in purple; (c) an eight-atom bulk fragment, shown in pink; (d) another nine-atom bulk fragment, shown in pink; (e) a six-atom bulk fragment, shown in red. The Si−Si and Ge−Ge bond lengths are 2.341 and 2.450 Å, respectively, and the bond angle is 109.47°.

calculated results, while the PBE results will also be presented for comparison. For germanium clusters, we adopted the PBE-calculated results.

III. Results and Discussion

Figure 1shows several bulk fragments (Si_9/Ge_9, Si_8/Ge_8, and Si_6/Ge_6) which are cut from a diamond Si or Ge structure. These bulk fragments are plotted as the references for bulk-like motifs appearing in the clusters which will be discussed later. The bond lengths are 2.341 and 2.450 Å, respectively, and bond angles are 109.47° for the diamond Si and Ge fragments plotted in Figure 1.

A. Lowest-Energy Structures of Si_n and Ge_n Clusters for $25 \leq n \leq 28$. The lowest-energy structures of silicon and germanium clusters ($n = 25-28$) are displayed in Figure 2. We can see from the B3LYP-calculated results that the lowest-energy structures of Si_{25-28} except for Si_{27} have a prolate shape in this size range, and the germanium clusters show also a prolate shape. The prolate shape of the silicon clusters contains a nine-atom fragment of diamond structure which is highlighted in purple (Figure 2). This Si_9 bulk motif connects to two small clusters Si_6 and Si_{10} to form the lowest-energy structure of Si_{25}. Si_{26} and Si_{28} can be viewed as the Si_9 unit connecting to two small clusters Si_7 and Si_{10} or Si_8 and Si_{10}, respectively. Note that the Si_6 (tetragonal bipyramid), Si_7 (pentagonal bipyramid), Si_9 (TTP), and Si_{10} (tetracapped trigonal prism) clusters are known to have special stabilities. The lowest-energy structure of Si_{27} is a Y-shaped structure, and it is formed by an assembly of a Si_8 bulk motif (highlighted in pink) and three stable clusters Si_6, Si_6, and Si_7. The total energy of the Y-shaped structure is only 0.042 eV lower than that of the prolate isomer of Si_{27} which is formed by a Si_9 unit connecting to two small clusters Si_8 and Si_{10}. However, from PBE calculations, only Si_{25} has a most stable prolate structure, and the lowest-energy structures of Si_{26}, Si_{27}, and Si_{28} are near-spherical cages with two, three, and two endohedral atoms, respectively. The PBE calculations predict a structural transition from prolate to cage at $n = 26$.

For germanium clusters in this size range, the lowest-energy structures of Ge_{25} and Ge_{26} have a similar pattern: an assembly of a Ge_6 bulk motif (highlighted in red) connecting to two small clusters of Ge_9 and Ge_{10} or Ge_{10} and Ge_{10}, respectively. On the other hand, Ge_{27} and Ge_{28} can be viewed as an assembly of a Ge_9 bulk motif connecting to a Ge_9 pair or Ge_9 and Ge_{10} clusters, respectively, similar to the cases of Si_{25}, Si_{26}, and Si_{28} from B3LYP calculations.

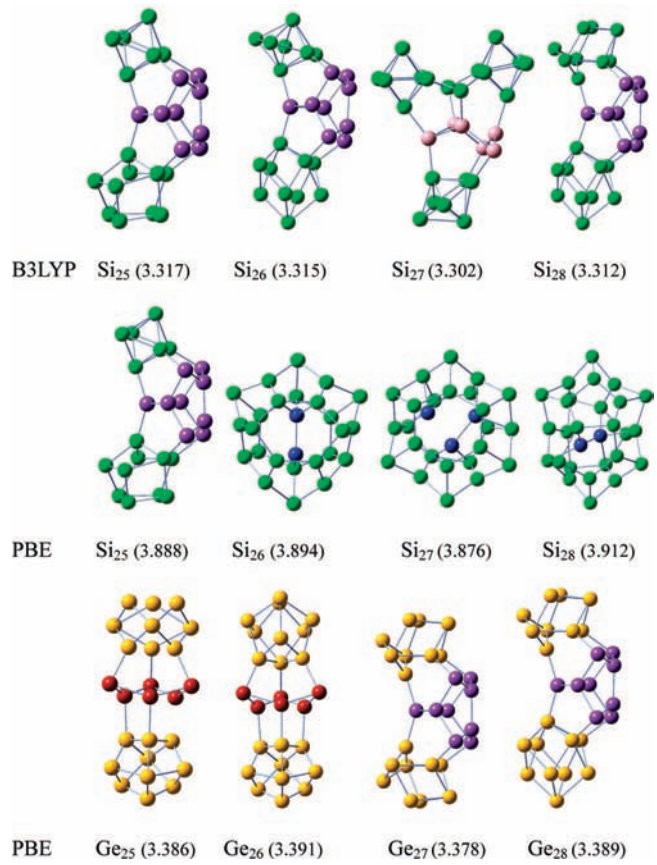

Figure 2. Lowest-energy isomers of silicon clusters (calculated at B3LYP/6-31G(d) and PBE/DND) and germanium clusters (calculated at PBE/DND) in the size range $25 \leq n \leq 28$, consistent with previously reported global minima.[32,39] The bulk fragments (Si_6/Ge_6, Si_8/Ge_8, and Si_9/Ge_9) are colored red, pink, and purple; endohedral atoms are in blue; and the attaching small clusters are in green and yellow for silicon and germanium, respectively. Values in parentheses are binding energies per atom in electronvolts.

The above B3LYP results for silicon clusters and PBE results for germanium clusters are consistent with the studies of Yoo et al.[32,33] By comparing the lowest-energy geometries of the silicon and germanium clusters with $25 \leq n \leq 28$, it can be found that all of these prolate and Y-shaped structures are formed by an assembly of a bulk motif of diamond structure and two or three small stable clusters. For silicon cluster structures with a prolate shape, they contain a Si_9 bulk motif; however, the Y-shaped structure of Si_{27} has a Si_8 bulk motif. The prolate structures of germanium clusters contain either a Ge_6 or a Ge_9 bulk fragment. For Ge_{25} and Ge_{26} the

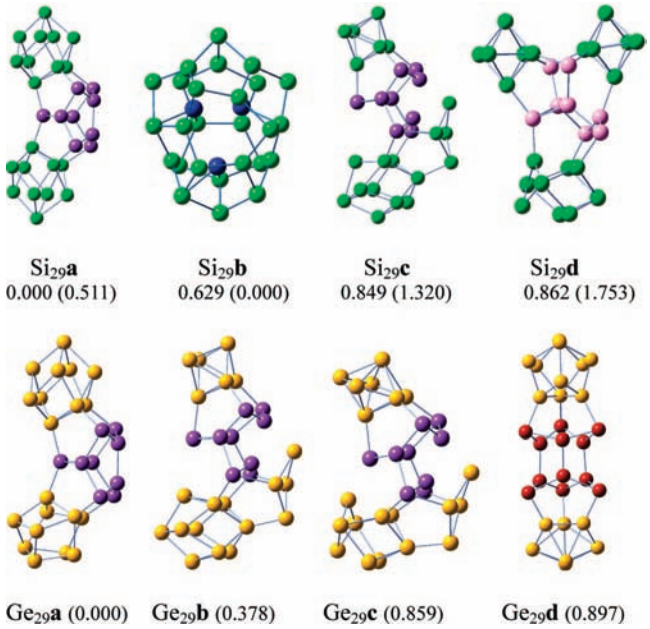

Figure 3. Low-lying isomers of Si_{29} and Ge_{29}. Relative energies (in eV) at B3LYP/6-31G(d) and PBE/DND (in parentheses) for Si_{29} and at PBE/DND for Ge_{29}. The lowest-energy isomers Si_{29}**a** and Ge_{29}**a** are consistent with the previously reported global minima.[32,39] Ge_{29}**b**, Ge_{29}**c**, and Ge_{29}**d** are new low-lying isomers we found in this work. The bulk fragments (Si_6/Ge_6, Si_8/Ge_8, and Si_9/Ge_9) are colored red, pink, and purple; endohedral atoms are in blue; and the attached small clusters are in green and yellow for silicon and germanium, respectively.

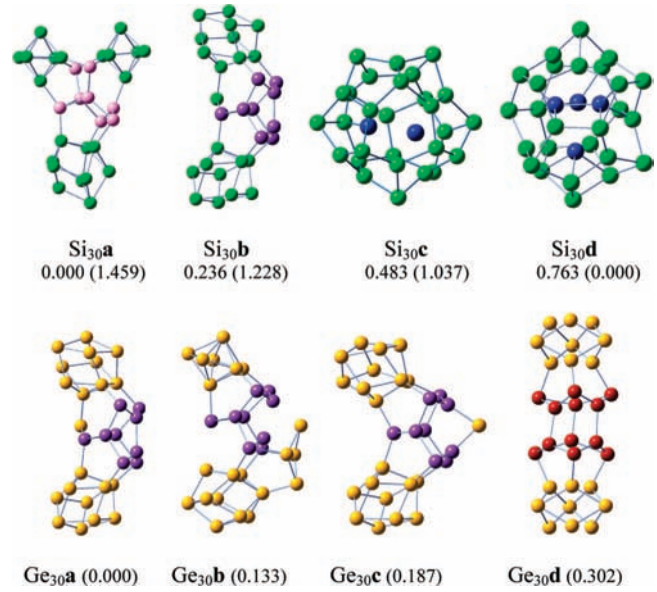

Figure 4. Low-lying energy isomers of Si_{30} and Ge_{30}. Relative energies (in eV) at B3LYP/6-31G(d) and PBE/DND (in parentheses) for Si_{30} and at PBE/DND for Ge_{30}. Si_{30}**a** is consistent with the previously reported global minimum.[32,34] Ge_{30}**a**, Ge_{30}**b**, Ge_{30}**c**, and Ge_{30}**d** are new structures obtained in this work. The bulk fragments (Si_6/Ge_6, Si_8/Ge_8, and Si_9/Ge_9) are colored red, pink, and purple; endohedral atoms are in blue; and the attached small clusters are in green and yellow for silicon and germanium, respectively.

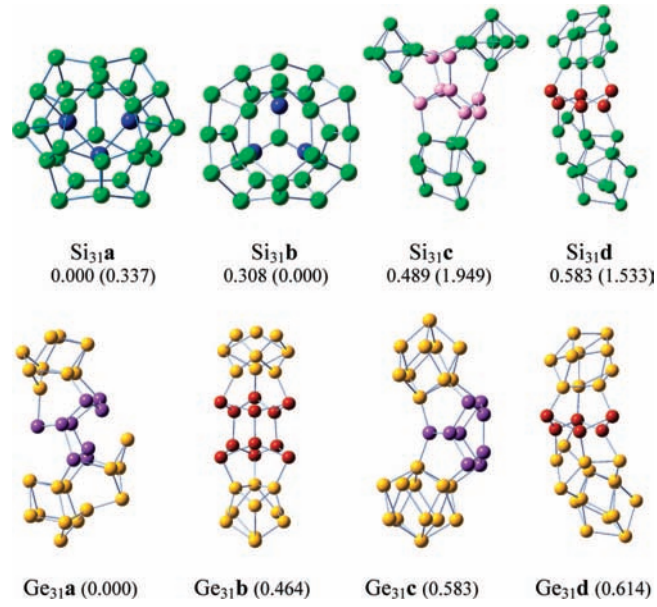

Figure 5. Low-lying isomers of Si_{31} and Ge_{31}. Relative energies (in eV) at B3LYP/6-31G(d) and PBE/DND (in parentheses) for Si_{31} and at PBE/DND for Ge_{31}. Si_{31}**a** is consistent with the previously reported global minimum.[33,34] Ge_{31}**a**, Ge_{31}**b**, Ge_{31}**c**, and Ge_{31}**d** are new structures obtained in this work. The bulk fragments (Si_6/Ge_6, Si_8/Ge_8, and Si_9/Ge_9) are colored red, pink, and purple; endohedral atoms are in blue; and the attached small clusters are in green and yellow for silicon and germanium, respectively.

lowest-energy isomers contain a Ge_6 bulk motif, whereas the lowest-energy structures of other clusters have a Ge_9 bulk motif. Ge_{25} and Ge_{26} keep the growth pattern of $Ge_{17,18,19,21,22,23}$ with a Ge_6 bulk motif connecting to two small clusters. When cluster size is larger, the lowest-energy structures contain a new bulk motif (Ge_9) from Ge_{27}.

B. Low-Lying Si_n and Ge_n Clusters for $n = 29-33$. The low-lying isomers of Si_n for $29 \leq n \leq 33$ are determined at the B3LYP/6-31G(d) and PBE/DND levels, respectively, and the low-lying isomers of Ge_n are obtained at the PBE/DND level. These isomers are shown in Figures 3, 4, 5, 6, and 7, in which Si_6, Si_8, and Si_9 bulk motifs (or Ge_6, Ge_8, and Ge_9 bulk motifs) are highlighted in red, pink, and purple, respectively, and the endohedral atoms are highlighted in blue.

The four low-lying isomers of Si_{29} and Ge_{29} are shown in Figure 3. The lowest-energy structure Si_{29}**a** calculated at B3LYP/6-31G(d) is formed by a Si_9 bulk unit connecting to two Si_{10}'s. Si_{29}**b** is a near-spherical cage with three endohedral atoms, which is the lowest-energy structure at PBE/DND. Si_{29}**c** is formed by a Si_9 bulk unit connecting to three clusters of Si_4 (a puckered rhombus), Si_6, and Si_{10}. This is a new growth pattern and is not referred to in previous studies. Si_{29}**d** is a Y-shaped structure assembled by a Si_8 bulk unit and three small clusters of Si_6, Si_6, and Si_9, in which the Si_6 pair locates on two sides of the Si_8 bulk unit. The prolate structures Ge_{29}**a** and Ge_{29}**b** are similar to Si_{29}**a** and Si_{29}**c**, respectively. Ge_{29}**c** is similar to Ge_{29}**b** but with a different set of small clusters (Ge_4, Ge_7, and Ge_9). Ge_{29}**d** contains a Ge_{12} unit (two symmetrical Ge_6 bulk units) which connects to two small clusters Ge_8 and Ge_9. We note that the low-lying isomers of Si_{29} contain three structural patterns (prolate, cage, and Y-shaped); however, Ge_{29} is mainly of prolate shape. We have calculated other structures of germanium clusters with near-spherical and Y-shaped patterns; however, they are more than 1.319 eV less stable than the prolate Ge_{29}**a**, indicating that the near-spherical and Y-shaped structures are less stable for Ge_{29}.

The Si_{30} and Ge_{30} are shown in Figure 4. Si_{30}**a** is a Y-shaped structure, which can be viewed as replacing a Si_9 cluster on the bottom of Si_{29}**d** by a Si_{10}. Si_{30}**b** is formed by adding one more atom to Si_{29}**a**. Si_{30}**c** and Si_{30}**d** are near-spherical cages with two and four endohedral atoms, respectively. At the B3LYP/6-31G(d) level, Si_{30}**a** (Y-shaped) is the lowest-energy structure.

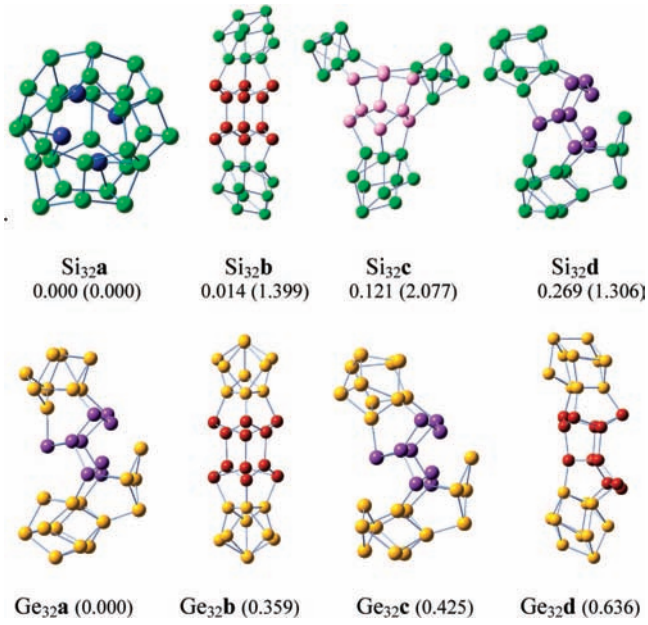

Figure 6. Low-lying isomers of Si_{32} and Ge_{32}. Relative energies (in eV) at B3LYP/6-31G(d) and PBE/DND (in parentheses) for Si_{32} and at PBE/DND for Ge_{32}. Si_{32}**a** is consistent with the previously reported global minimum.[33,34] Ge_{32}**a**, Ge_{32}**b**, Ge_{32}**c**, and Ge_{32}**d** are new structures obtained in this work. The bulk fragments (Si_6/Ge_6, Si_8/Ge_8, and Si_9/Ge_9) are colored red, pink, and purple; endohedral atoms are in blue; and the attached small clusters are in green and yellow for silicon and germanium, respectively.

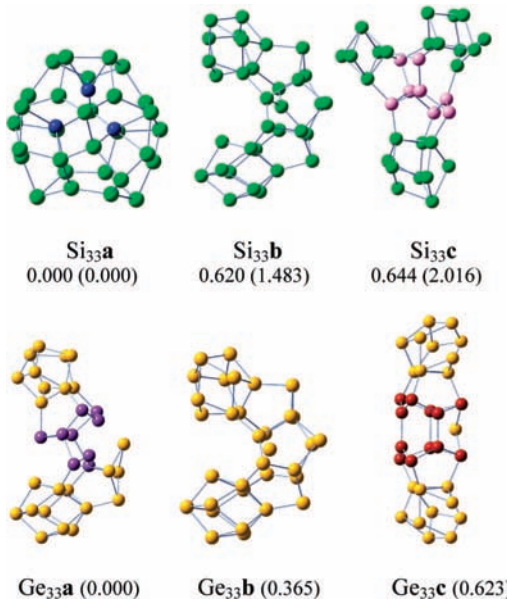

Figure 7. Low-lying isomers of Si_{33} and Ge_{33}. Relative energies (in eV) at B3LYP/6-31G(d) and PBE/DND (in parentheses) for Si_{33} and at PBE/DND for Ge_{33}. Si_{33}**a** is consistent with the previously reported global minimum.[33,34] Ge_{33}**a**, Ge_{33}**b**, Ge_{33}**c**, and Ge_{33}**d** are new structures obtained in this work. The bulk fragments (Si_6/Ge_6, Si_8/Ge_8, and Si_9/Ge_9) are colored red, pink, and purple; endohedral atoms are in blue; and the attached small clusters are in green and yellow for silicon and germanium, respectively.

However, at the PBE/DND level, Si_{30}**c** and Si_{30}**d** (cages) are shown as dominant structures for Si_{30}. The lowest-energy isomer Ge_{30}**a** is a prolate structure similar to Si_{30}**b**. Ge_{30}**b** and Ge_{30}**d** keep the growth patterns of Ge_{29}**b** and Ge_{29}**d**, respectively. The low-lying isomers of Ge_{30} are of prolate shape, and the order of stability is consistent with Ge_{29}. For Si_{30} there are several kinds of shapes (Y-shape, prolate, and cage) in the low-lying isomers and the order of stability is different from Si_{29} at the B3LYP/6-31G(d) level. These results indicate that the growth patterns of germanium and silicon clusters may have a considerable deviation at this size.

For Si_{31} and Ge_{31}, the feature of the lowest-energy structures is completely different. As shown in Figure 5. The lowest-energy isomer Si_{31}**a** and the second lowest-energy isomer Si_{31}**b** are cages with three endohedral atoms. We note that these cage isomers are also favored at the PBE level. Si_{31}**c** is a Y-shaped structure, and Si_{31}**d** is formed by a Si_6 bulk unit connecting with two Si_{10}'s and five additional atoms. The lowest-energy structure Ge_{31}**a** is formed by a Ge_9 bulk unit connecting with a Ge_4 and two Ge_9's, similar to Ge_{30}**b**. Ge_{31}**d** is similar to Si_{31}**d**. Other isomers of Ge_{31} are also displayed in Figure 5. In this size, the structures of silicon and germanium clusters are very different: the endohedral cages are shown as dominant patterns for silicon clusters, whereas the lowest-energy structure of Ge_{31} still keep a prolate shape but a new type. Hence, the growth trends for $Si_{30} \rightarrow Si_{31}$ and $Ge_{30} \rightarrow Ge_{31}$ are different.

As shown in Figure 6, the structural patterns of the lowest-energy isomers of Si_{32} and Ge_{32} are the same those of as Si_{31} and Ge_{31}, respectively. For Si_{32} the cage structure with four endohedral atoms (Si_{32}**a**) is the most stable based on both PBE and B3LYP calculations. Si_{32}**c** has a Y-shaped geometry, similar to Si_{31}**c**, but with a Si_9 bulk motif rather than a Si_8 bulk motif. The prolate Ge_{32}**a** is similar to Ge_{31}**a**, and Ge_{32}**c** and Si_{32}**d** are similar to Ge_{32}**a** with only a difference in the positions of Ge_{10} (or Si_{10}) and Ge_9 (or Si_9). Ge_{32}**d** exhibits a new growth pattern, which is formed by a Ge_{10} pair connected via a Ge_{12} unit (two opposite Ge_6 bulk motifs).

In Figure 7, we show the low-lying isomers of Si_{33} and Ge_{33}. The patterns for these structures are similar to Si_{32} and Ge_{32} as discussed in the above paragraph except for Si_{33}**b** and Ge_{33}**b**, which are packed by a Si_{11} (or Ge_{11}) and two Si_{10} (or Ge_{10}) clusters with two link atoms.

From Si_{29} to Si_{33}, the shape of the B3LYP/6-31G(d) lowest-energy structure undergoes a transition from prolate to Y-shaped and then to cage structure. Si_{31} can be considered a point of structural transition to cage. Based on the PBE-calculated results, such a transition occurs at Si_{26}. Both the B3LYP and PBE results are consistent with the experimental prediction of this transition at the size range of 24–34.[19] From Ge_{29} to Ge_{33}, all the lowest-energy structures have prolate shape. Ge_{29} and Ge_{30} belong to the same prolate type that is constructed by a Ge_9 unit connecting with two small clusters; $Ge_{31}-Ge_{33}$ belong to another prolate type that is assembled by a Ge_9 unit connecting with three small clusters including a Ge_4 cluster and such prolate structures start to show dish-like tendency.

We note that at $25 \leq n \leq 33$ Si_n cluster exhibits a transition from the prolate to a spherical shape while such a transition does not occur for Ge_n clusters in the same size range. In order to explain the different growth patterns of Si_n and Ge_n ($n = 25-33$) clusters, we have calculated the relative energies of the small Si_n and Ge_n clusters (Si_{10}, Si_7, Si_6, Ge_{10}, Ge_7, and Ge_6) with respect to the bulk diamond structures of silicon and germanium, respectively. As one can see from the results shown in Table 2, the small clusters Ge_{10}, Ge_7, and Ge_6 can acquire about 85, 82, and 79% of their bulk energy, while the corresponding small Si_n clusters can only get about 80, 77, and 71% of their bulk energy. These results may be attributed to the more metallic bonding nature in Ge than in Si. These results also indicate that the building blocks of 6-, 7-, and particularly 10-atom clusters for the medium-sized clusters are energetically more favorable in Ge than in Si. Therefore, one would expect

TABLE 2: Binding Energies per Atom of Si_6, Si_7, and Si_{10} and Ge_6, Ge_7, and Ge_{10} Compared with Si and Ge Diamond Structures at the PBE/DND Level

	binding energy (eV/atom)	Si_n/Si(bulk) (%)		binding energy (eV/atom)	Ge_n/Ge(bulk) (%)
Si_6	3.3468	71	Ge_6	3.092	79
Si_7	3.6097	77	Ge_7	3.208	82
Si_{10}	3.7599	80	Ge_{10}	3.316	85
Si(bulk)	4.6866	100	Ge(bulk)	3.909	100

the transition from the $Si_{6,7,10}$ or $Ge_{6,7,10}$ stacking pattern to a more spherical motif to happen earlier in Si_n clusters since the building blocks for the stacking pattern in Si_n clusters cost more than in Ge_n clusters. The appearance of a new growth pattern for Ge_n clusters around $n = 31$, i.e., a bulk motif connecting to two small clusters and a Ge_4 fragment, also suggests that small cluster blocks tend to pack in two-dimensional (2-D) rather than the initial one-dimensional growth motif at smaller size range. The 2-D growth pattern will gain more interactions between the building blocks and lower the cluster's total energy. This growth trend in Ge_n clusters is consistent with experimental mobility measurements.[8] It was found by experiment that Ge_n clusters will not grow into the more spherical shape until the size range of 64–76.[8]

From the above discussions, we see that the prolate and Y-shaped cluster structures usually contain several building blocks including a small bulk-like fragment and small clusters. We have also examined the bond lengths between the atoms within individual building block and the atoms between different building blocks, and we found that they are similar without obvious differences. As shown in Figure 1, the buckled-hexagonal ring is an important feature of the bulk fragments of Si_9/Ge_9, Si_8/Ge_8, and Si_6/Ge_6. When the bulk fragment is embedded in the cluster, noticeable distortions have been observed. As shown in Figure 8a, the buckled-hexagonal ring connects to two small clusters through sharing the two triangular faces (Δ135 and Δ246). Three distant atoms 1, 3, and 5 in the buckled-hexagonal ring are found to approach each other when the ring is embedded in the clusters. This distortion causes three bond angles ($\angle$214, $\angle$456, and $\angle$632) to increase and the other three bond angles ($\angle$145, $\angle$563, and $\angle$321) to decrease, compared to the bond angles in the perfect bulk fragment. The small clusters in prolate and Y-shaped medium-sized clusters are those with size $n = 4$, 6, 7, 9, and 10, respectively. These small clusters also often undergo distortion or even transformation compared to their free-standing form. Some common changes in the small cluster structures are shown in Figure 8. The free Si_4/Ge_4 cluster is a plane rhombus; however, in bigger clusters it is slightly buckled. For $n = 6$ and 7, the shapes of small clusters have no obvious changes when acting as building blocks. However, for Si_9/Ge_9 and Si_{10}/Ge_{10}, their stacking patterns changes from (1,4,4) → (3,3,3) and (1,3,3,3) → (1,4,4,1), respectively, when they are incorporated into the medium-sized clusters. These changes of small cluster structures have a common feature, namely, the surfaces of clusters tend to form buckled rhombuses (similar to Si_4/Ge_4 in Figure 8b). The buckled-rhombus surfaces can be favorable interfaces with other blocks since they can be considered favorable bulk fragments.

C. Relative Stabilities. The binding energies per atom, second differences of cluster energies, and the HOMO–LUMO gaps as a function of cluster size are plotted in Figure 9, and total energy differences, binding energies, and HOMO–LUMO gaps are also listed in Tables 3 and 4. The binding energy per atom is defined by $E_b = [nE_{atom} - E_{total}]/n$, in which E_{total} and E_{atom} are energies of the cluster and ground state of a free atom, respectively. Here, for Si clusters, we list two sets of relative energies, binding energies, and HOMO–LUMO gaps at the B3LYP/6-31G(d) and PBE/DND levels, respectively. For each size of clusters, the calculated lowest-energy isomers are denoted by the number 0.000 in Tables 3 and 4.

In Figure 9a, we have shown the B3LYP binding energy curve of lowest-energy silicon clusters. The tendency of the present binding energy curve is in agreement with previous studies.[32] The binding energy curve of Ge_n clusters is shown in Figure 9b; the tendency of the curve increases gradually with cluster size, and Ge_{29} also corresponds to a local maximum. On the other hand, Ge_{27} and Ge_{30} clusters correspond to local minima in the binding energy curve. These results suggest Si_{29} and Ge_{29} have special stability, and Ge_{27} and Ge_{30} have less stability.

The relative cluster stabilities can be also estimated through second-order difference of total energy, as shown in Figure 9c,d, which is a sensitive quantity that can characterize the stabilities of clusters. We note that the trends of the second-order differences in energies are very similar for the silicon and

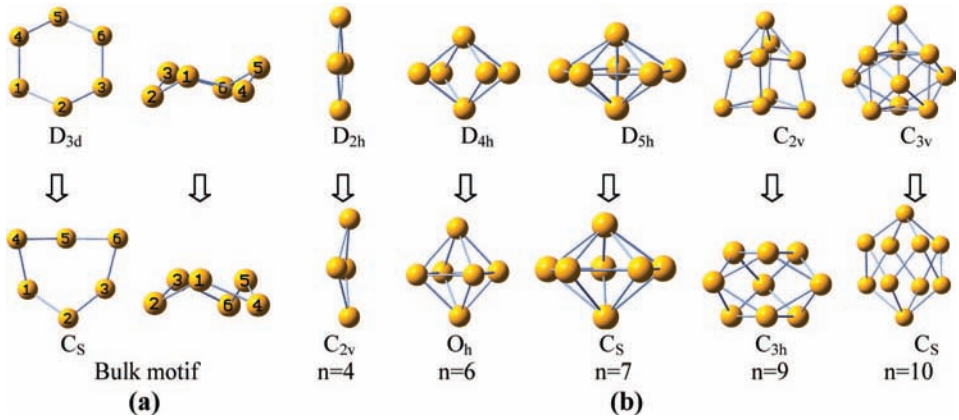

Figure 8. Structural changes of a Si_6/Ge_6 bulk motif and small Si_n/Ge_n clusters from free-standing to building blocks in large clusters.

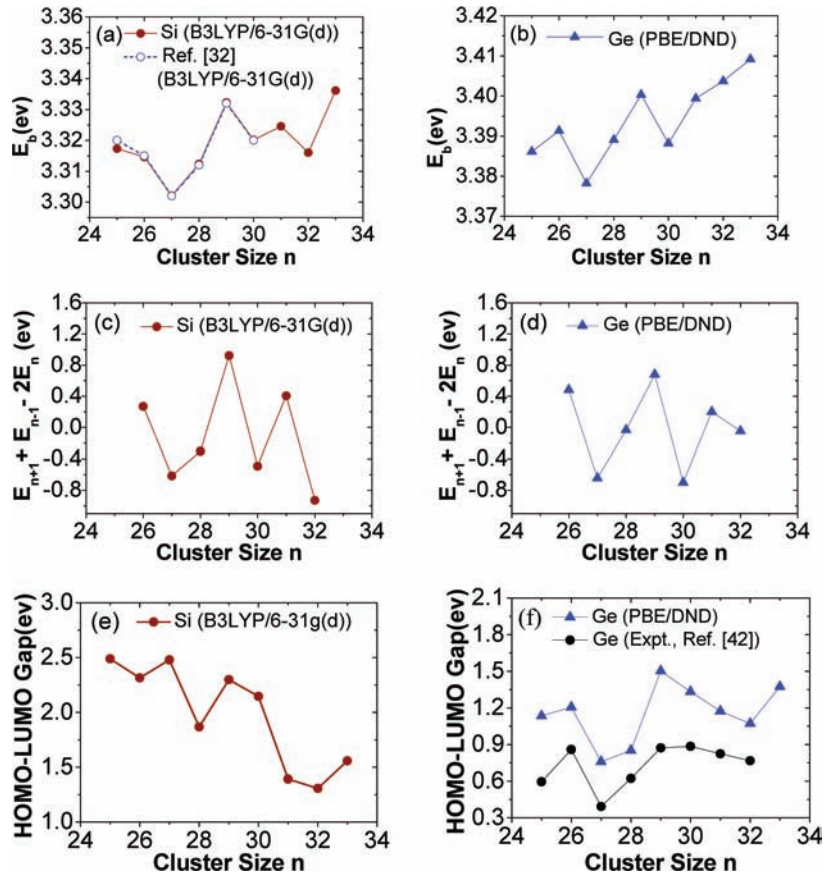

Figure 9. (a) Binding energies per atom of lowest-energy Si_n ($n = 25-33$) clusters at B3LYP/6-31G(d). (b) Binding energies per atom of lowest-energy Ge_n ($n = 25-33$) isomers at the PBE/DND level. (c, d) Second-order differences in energies, defined by $\Delta_2E(n) = E(n+1) + E(n-1) - 2E(n)$ as a function of cluster size n, for lowest-energy Si_n and Ge_n clusters, respectively. (e, f) HOMO–LUMO gaps of lowest-energy Si_n and Ge_n clusters versus cluster size n, respectively.

TABLE 3: Relative Energies (ΔE) with Respect to the Lowest-Energy Isomers, Binding Energies (E_b) per Atom, and HOMO−LUMO Gaps of Low-Lying Isomers

	Gaussian 03/B3LYP/6-31G(d)			DMol3/PBE/DND		
	ΔE (eV)	E_b (eV/atom)	gap (eV)	ΔE (eV)	E_b (eV/atom)	gap (eV)
Si_{29}**a**	**0.000**	3.332	2.299	0.511	3.915	1.469
Si_{29}**b**	0.629	3.311	1.773	**0.000**	3.932	0.814
Si_{29}**c**	0.849	3.303	2.066	1.320	3.887	1.252
Si_{29}**d**	0.862	3.303	1.548	1.753	3.872	0.879
Si_{30}**a**	**0.000**	3.320	2.147	1.459	3.885	1.385
Si_{30}**b**	0.236	3.312	2.368	1.228	3.893	1.434
Si_{30}**c**	0.483	3.304	1.602	1.037	3.900	0.721
Si_{30}**d**	0.763	3.295	1.439	**0.000**	3.934	0.702
Si_{31}**a**	**0.000**	3.325	1.392	0.337	3.928	0.446
Si_{31}**b**	0.308	3.315	1.602	**0.000**	3.939	0.852
Si_{31}**c**	0.489	3.309	2.180	1.949	3.876	1.380
Si_{31}**d**	0.583	3.308	2.166	1.533	3.889	1.295
Si_{32}**a**	**0.000**	3.316	1.307	**0.000**	3.945	0.514
Si_{32}**b**	0.014	3.316	1.394	1.399	3.901	0.525
Si_{32}**c**	0.121	3.312	1.852	2.077	3.880	0.945
Si_{32}**d**	0.269	3.308	1.873	1.306	3.904	1.067
Si_{33}**a**	**0.000**	3.336	1.558	**0.000**	3.957	0.710
Si_{33}**b**	0.620	3.317	2.036	1.483	3.912	1.108
Si_{33}**c**	0.644	3.317	1.776	2.016	3.896	1.026

TABLE 4: Relative Energies (ΔE) with Respect to the Lowest-Energy Isomers, Binding Energies (E_b) per Atom, and HOMO−LUMO Gaps of Low-Lying Isomers

	DMol3/PBE/DND		
	ΔE (eV)	E_b (eV/atom)	gap (eV)
Ge_{29}**a**	**0.000**	3.400	1.502
Ge_{29}**b**	0.378	3.387	1.331
Ge_{29}**c**	0.859	3.371	0.971
Ge_{29}**d**	0.897	3.369	0.645
Ge_{30}**a**	**0.000**	3.388	1.333
Ge_{30}**b**	0.133	3.384	1.167
Ge_{30}**c**	0.187	3.382	1.015
Ge_{30}**d**	0.302	3.378	0.512
Ge_{31}**a**	**0.000**	3.399	1.173
Ge_{31}**b**	0.464	3.384	0.558
Ge_{31}**c**	0.583	3.381	1.521
Ge_{31}**d**	0.614	3.380	1.132
Ge_{32}**a**	**0.000**	3.404	1.072
Ge_{32}**b**	0.359	3.392	0.541
Ge_{32}**c**	0.425	3.390	0.732
Ge_{32}**d**	0.636	3.384	0.936
Ge_{33}**a**	**0.000**	3.409	1.374
Ge_{33}**b**	0.365	3.398	1.105
Ge_{33}**c**	0.623	3.390	1.086

germanium clusters, despite their growth patterns being much different. Local maximum peaks are found at $n = 29$ and 31, indicating that clusters with these sizes are more stable than their neighboring clusters.

We also compared the energy gaps between the highest occupied molecular orbits (HOMOs) and lowest unoccupied molecular orbits (LUMOs) for the lowest-energy structures of Si_n and Ge_n ($n = 25-33$) clusters. From Figure 9e and Table 3, we can see that all of near-spherical silicon clusters have small HOMO–LUMO gaps compared with prolate and Y-shape isomers from both B3LYP and PBE calculations. At the B3LYP level, Si_{31-33} (cage shape) display relatively small HOMO–LUMO gaps. In Figure 9f, the HOMO–LUMO gaps of Ge_n clusters

from this work and experiments[42] are compared. The tendency of the calculated HOMO–LUMO gap curve is consistent with the experimental result. While the HOMO–LUMO gap curves of silicon and germanium clusters are much different, both show a local maximum at $n = 29$, indicating the good chemical stabilities of Si_{29}**a**, Si_{29}**b**, and Ge_{29}**a**. Si_{33} and Ge_{33}, with large binding energies, also display relatively large HOMO–LUMO gaps. Note that there is not always a strong correlation between binding energy and HOMO–LUMO gap. In Table 3, we can see that Si_{31}**a**, Si_{32}**a**, and Si_{33}**a** have large binding energies, but relatively small HOMO–LUMO gaps, compared to Si_{31}**d**, Si_{32}**d**, and Si_{33}**b**, which have relatively small binding energies but large HOMO–LUMO gaps. The binding energies can be considered to reveal thermodynamic stability, and the HOMO–LUMO gaps show potential chemical reactivity. However, they have no direct relationship. The HOMO–LUMO gap would correlate with the geometry of a cluster, because similar structural motifs can result in similar electronic distributions. Si_{31}**a**, Si_{32}**a**, and Si_{33}**a** are all endohedral cages; as a result, they have relatively small HOMO–LUMO gaps compared to other isomers. On the other hand, Ge_{29}**a**, Ge_{30}**a**, and Ge_{31}**c** belong to the same pattern of prolate geometry with a Ge_9 motif; they show the maximal HOMO–LUMO gap compared to other isomers. These results suggest that the HOMO–LUMO gap has a close correlation with the geometry configuration of a cluster.

IV. Conclusion

We have performed global structural optimizations for Si_n and Ge_n neutral clusters in the $25 \leq n \leq 33$ size range. The low-lying isomers of Si_n and Ge_n are obtained based on GA search combined with DFT calculations. Since silicon clusters have evident functional dependence, and germanium clusters almost have not, DFT calculations with both B3LYP and PBE functionals were performed for Si_n, and only the PBE functional was used in the DFT calculations for Ge_n. Our approach based on the B3LYP functional reproduces well the lowest-energy structures of Si_n compared to previous studies, and before Ge_{29} the lowest-energy structures of Ge_n are also consistent with previous studies, demonstrating the accuracy and reliability of our approach. Our present study pays more attention to determining low-lying isomers of Ge_n ($n = 29-33$) and studying the growth patterns of Si_n and Ge_n ($n = 25-33$) clusters.

In the size range $25 \leq n \leq 33$, the low-lying isomers of germanium clusters display prolate shapes, whereas the corresponding silicon clusters have versatile character containing three types of geometries in the low-lying isomers, namely, prolate, near-spherical, and Y-shaped. The prolate and Y-shaped geometries are formed via a fragment of bulk diamond structure (Si_6, Si_9, and Si_8 units or Ge_6, Ge_9, and Ge_8 units) connecting with two or three small clusters. The near-spherical geometries are endohedral cages. For $Si_{25}-Si_{30}$, the B3LYP calculations suggest that the prolate and Y-shaped structures as assembled by small clusters and bulk motifs are very competitive for the global minima, and the growth patterns of Si_n clusters undergo a transition from prolate and Y-shaped to cage structure around $n = 31$. Si_{31} can be considered the transition point from Y-shaped to cage structure. However, the PBE calculation results suggest that near-spherical clusters are very competitive to be the global minima in the size range $n = 26-33$, and the transition of the growth pattern from prolate to cage appears at $n = 26$. The prolate structures for germanium clusters with $n = 25-33$ have also experienced changes in prolate patterns. For 25 and 26, Ge_n clusters are assembled by a Ge_6 bulk motif connecting to two small clusters. From 27 to 30, Ge_n clusters are formed by a Ge_9 unit connecting with two small clusters. From 31 to 33, Ge_n clusters are formed by a Ge_9 unit connecting with three small clusters including a Ge_4 fragment, making the Ge_n cluster a little dish-like. The growth patterns of Si_n and Ge_n clusters display a large deviation in the size range $25 \leq n \leq 33$. By analyzing the properties of Si_n and Ge_n with $n = 25-33$, we note that Si_n and Ge_n with $n = 29$ reveal special stabilities.

In this paper, we also explained the different growth patterns of Si_n and Ge_n clusters with $n = 25-33$ according to the analyses on the relative energies of the small Si_n and Ge_n clusters (Si_{10}, Si_7, Si_6, Ge_{10}, Ge_7, and Ge_6) with respect to the bulk Si and bulk Ge, respectively. The calculated results indicate that the building blocks of 6-, 7-, and particularly 10-atom clusters for the medium-sized clusters is energetically more favorable in Ge than in Si. Therefore, the transition from the $Si_{6,7,10}$ or $Ge_{6,7,10}$ stacking pattern to a more spherical motif would happen earlier in Si_n clusters than in Ge_n clusters. We also note that when small clusters serve as building blocks of bigger clusters, their surfaces tend to show puckered rhombuses which might be favorable interfaces for clusters' aggregation and can also lead to bulk-motif linking with other blocks.

Acknowledgment. This work was supported by the National Natural Science Foundation of China (Nos. 20473030, 20773047, and 60028403). Ames Laboratory is operated for the U.S. Department of Energy by Iowa State University under Contract No. DE-AC02-07CH11358. This work was also supported by the Director for Energy Research, Office of Basic Energy Sciences.

References and Notes

(1) Gingerich, K. A.; Schmude, R. W., Jr.; Baba, M. S.; Meloni, G. *J. Chem. Phys.* **2000**, *112*, 7443.
(2) Martin, T. P.; Schaber, H. *J. Chem. Phys.* **1985**, *83*, 855.
(3) Phillips, J. C. *J. Chem. Phys.* **1986**, *85*, 5246.
(4) Schulze, W.; Winter, B.; Goldenfeld, I. *J. Chem. Phys.* **1987**, *87*, 2402.
(5) Heath, J. R.; Liu, Y.; O'Brien, S. C.; Zhang, Q. L.; Curl, R. F.; Tittel, F. K.; Smalley, R. E. *J. Chem. Phys.* **1985**, *83*, 5520.
(6) Yoshida, S.; Fuke, K. *J. Chem. Phys.* **1999**, *111*, 3880.
(7) Burton, G. R.; Xu, C. S.; Arnold, C. C.; Meumark, D. M. *J. Chem. Phys.* **1996**, *104*, 2757.
(8) Hunter, J. M.; Fye, J. L.; Jarrold, M. F.; Bower, J. E. *Phys. Rev. Lett.* **1993**, *73*, 2063.
(9) Alford, J. M.; Laaksonen, R. T.; Smalley, R. E. *J. Chem. Phys.* **1991**, *94*, 2618.
(10) Shvartsburg, A. A.; Liu, B.; Lu, Z. Y.; Wang, C. Z.; Jarrold, M. F.; Ho, K. M. *Phys. Rev. Lett.* **1999**, *83*, 2167.
(11) Shvartsburg, A. A.; Hudgins, R. R.; Dugourdb, P.; Jarrold, M. F. *Chem. Soc. Rev.* **2001**, *30*, 26.
(12) Marsen, B.; Lonfat, M.; Scheier, P.; Sattler, K. *Phys. Rev. B* **2000**, *62*, 6892.
(13) Ray, U.; Jarrold, M. F. *J. Chem. Phys.* **1991**, *94*, 2631.
(14) Bergeron, D. E.; Castleman, A. W., Jr *J. Chem. Phys.* **2002**, *117*, 3219.
(15) Jarrold, M. F.; Ijiri, Y.; Ray, U. *J. Chem. Phys.* **1991**, *94*, 3607.
(16) Jarrold, M. F.; Ijiri, Y.; Constant, V. A. *Phys. Rev. Lett.* **1991**, *67*, 2994.
(17) Schäfer, R.; Schlecht, S.; Woenckhaus, J.; Becker, J. A. *Phys. Rev. Lett.* **1996**, *76*, 471.
(18) Jarrold, M. F.; Honea, E. C. *J. Phys. Chem.* **1991**, *95*, 9181.
(19) Jarrold, M. F.; Bower, J. E. *J. Chem. Phys.* **1992**, *96*, 9180.
(20) Hudgins, R. R.; Imai, M.; Jarrold, M. F. *J. Chem. Phys.* **1999**, *111*, 7865.
(21) Zhang, Q. L.; Liu, Y.; Curl, R. F.; Tittle, F. K.; Smalley, R. E. *J. Chem. Phys.* **1988**, *88*, 1670.
(22) Fuke, K.; Tsukamoto, K.; Misaizu, F.; Sanekata, M. *J. Chem. Phys.* **1993**, *99*, 7807.
(23) Yoshida, S.; Fuke, K. *J. Chem. Phys.* **1999**, *111*, 3880.
(24) Mitas, L.; Grossman, J. C.; Stich, I.; Tobik, J. *Phys. Rev. Lett.* **2000**, *84*, 1479.
(25) Yoo, S.; Zeng, X. C. *Angew. Chem., Int. Ed.* **2005**, *44*, 1491.
(26) Goedecker, S.; Hellmann, W. *Phys. Rev. Lett.* **2005**, *95*, 055501.

(27) Sieck, A.; Frauenheim, Th.; Jackson, K. A. *Phys. Status Solidi B* **2003**, *240*, 537.
(28) Jackson, K. A.; Horoi, M. H. *Phys. Rev. Lett.* **2004**, *93*, 013401.
(29) Yoo, S.; Zeng, X. C.; Zhu, X. L.; Bai, J. *J. Am. Chem. Soc.* **2003**, *125*, 13318.
(30) Yoo, S.; Zhao, J. J.; Wang, J. L.; Zeng, X. C. *J. Am. Chem. Soc.* **2004**, *126*, 13845.
(31) Bai, J.; Cui, L. F.; Wang, J. L.; et al. *J. Phys. Chem. A* **2006**, *110*, 908.
(32) Yoo, S.; Zeng, X. C. *J. Chem. Phys.* **2006**, *124*, 054304.
(33) Yoo, S.; Shao, N.; Koehler, C.; Fraunhaum, T.; Zeng, X. C. *J. Chem. Phys.* **2006**, *124*, 164311.
(34) Oña, O.; Bazterra, V. E.; Caputo, M. C.; Facelli, J. C.; Fuentealba, P.; Ferraro, M. B. *Phys. Rev. A* **2006**, *73*, 063203.
(35) Busulu, S.; Yoo, S.; Zeng, X. C. *J. Chem. Phys.* **2005**, *122*, 164305.
(36) Wang, J. L.; Wang, G. H.; Zhao, J. J. *Phys. Rev. B* **2001**, *64*, 205411.
(37) Ma, S. J.; Wang, G. H. *THEOCHEM* **2006**, *767*, 75.
(38) Liang, F. S.; Li, B. X. *Phys. Lett. A* **2004**, *328*, 407.
(39) Yoo, S.; Zeng, X. C. J. *Chem. Phys.* **2006**, *124*, 184309.
(40) Frisch, M. J.; Trucks, G. W.; Schlegel, H. B.; Scuseria, G. E.; Robb, M. A.; Cheeseman, J. R.; Montgomery, J. A., Jr.; Vreven, T.; Kudin, K. N.; Burant, J. C.; Millam, J. M.; Iyengar, S. S.; Tomasi, J.; Barone, V.; Mennucci, B.; Cossi, M.; Scalmani, G.; Rega, N.; Petersson, G. A.; Nakatsuji, H.; Hada, M.; Ehara, M.; Toyota, K.; Fukuda, R.; Hasegawa, J.; Ishida, M.; Nakajima, T.; Honda, Y.; Kitao, O.; Nakai, H.; Klene, M.; Li, X.; Knox, J. E.; Hratchian, H. P.; Cross, J. B.; Bakken, V.; Adamo, C.; Jaramillo, J.; Gomperts, R.; Stratmann, R. E.; Yazyev, O.; Austin, A. J.; Cammi, R.; Pomelli, C.; Ochterski, J. W.; Ayala, P. Y.; Morokuma, K.; Voth, G. A.; Salvador, P.; Dannenberg, J. J.; Zakrzewski, V. G.; Dapprich, S.; Daniels, A. D.; Strain, M. C.; Farkas, O.; Malick, D. K.; Rabuck, A. D.; Raghavachari, K.; Foresman, J. B.; Ortiz, J. V.; Cui, Q.; Baboul, A. G.; Clifford, S.; Cioslowski, J.; Stefanov, B. B.; Liu, G.; Liashenko, A.; Piskorz, P.; Komaromi, I.; Martin, R. L.; Fox, D. J.; Keith, T.; Al-Laham, M. A.; Peng, C. Y.; Nanayakkara, A.; Challacombe, M.; Gill, P. M. W.; Johnson, B.; Chen, W.; Wong, M. W.; Gonzalez, C.; Pople, J. A. *Gaussian 03*, revision B; Gaussian, Inc.: Pittsburgh, PA, 2003.
(41) (a) Delley, B. *J. Chem. Phys.* **1990**, *92*, 508. (b) Delley, B. *J. Chem. Phys.* **1991**, *94*, 7245.
(42) Negishi, Y.; Kawamata, H.; Nakajima, A.; Kaya, K. *Chem. Phys. Lett.* **1998**, *294*, 370.

JP710937M